CHEMISTRY OF MATERIALS

ARTICLE

pubs.acs.org/cm

Preparation, Characterization, and Photoluminescence Properties of Tb^{3+}-, Ce^{3+}-, and Ce^{3+}/Tb^{3+}-Activated $RE_2Si_4N_6C$ (RE = Lu, Y, and Gd) Phosphors

Chengjun Duan,*[,†] Zhijun Zhang,[‡] Sven Rösler,[†] Sylke Rösler,[†] Anneke Delsing,[§] Jingtai Zhao,[‡] and H. T. Hintzen[§]

[†]Leuchtstoffwerk Breitungen GmbH, Lange Sömme 17, D-98597 Breitungen, Germany

[‡]Key Laboratory of Transparent Opto-Functional Inorganic Materials of Chinese Academy of Sciences, Shanghai Institute of Ceramics, Shanghai, 200050, People's Republic of China

[§]Eindhoven University of Technology, P.O. Box 513, 5600 MB Eindhoven, The Netherlands

Supporting Information

ABSTRACT: Photoluminescence properties of Tb^{3+} and Ce^{3+} singly doped and Ce^{3+}/Tb^{3+}-codoped $RE_2Si_4N_6C$ (RE = Lu, Y, and Gd) phosphors were investigated. Tb^{3+} shows similar luminescence properties in $RE_2Si_4N_6C$ (RE = Lu, Y, and Gd) host lattices and emits bright green light under UV excitation around 300 nm. The luminescence properties of Ce^{3+} in $RE_2Si_4N_6C$ host lattices are influenced by the size of the RE^{3+} ions ($Lu_2Si_4N_6C$ and $Y_2Si_4N_6C$ vs $Gd_2Si_4N_6C$). Both Ce^{3+}-activated $Lu_2Si_4N_6C$ and $Y_2Si_4N_6C$ phosphors exhibit a broad band emission in the wavelength range of 450−750 nm with peak center at about 540 nm, while Ce^{3+}-activated $Gd_2Si_4N_6C$ shows a broad emission band in the wavelength range of 500−800 nm with peak center at about 610 nm. This difference is ascribed to the different site occupations of Ce^{3+} on the two crystallographic sites in $Gd_2Si_4N_6C$ as compared to the Y and Lu compounds. In Ce^{3+}/Tb^{3+}-codoped $RE_2Si_4N_6C$ (RE = Lu, Y, and Gd) phosphors, it is observed that energy transfer takes place from Ce^{3+} to Tb^{3+} in Ce^{3+}/Tb^{3+}-codoped $Lu_2Si_4N_6C$ and $Y_2Si_4N_6C$ but in the reversed direction from Tb^{3+} to Ce^{3+} in Ce^{3+}/Tb^{3+}-codoped $Gd_2Si_4N_6C$, depending on the position of the 5d level of Ce^{3+} versus the $^5D_4$ level of Tb^{3+}. The potential applications of these phosphors are pointed out.

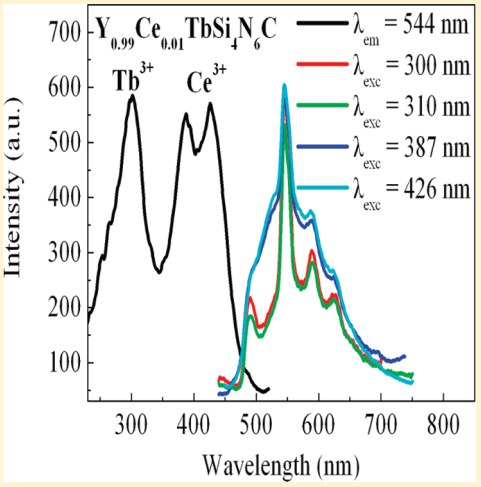

KEYWORDS: optical materials, characterization of materials, inorganic solids and ceramics

1. INTRODUCTION

Recently, several quaternary rare-earth containing silicon−nitride−carbides, $RE_2Si_4N_6C$ (RE = Y, Ho, Tb, and La), have been found and characterized.[1−6] Structurally, they are derived from the quaternary silicon nitride compounds, $MRESi_4N_7$ (M = Ba, Sr, Ca, Eu; RE = Y, Yb),[7−14] by formal substitutions of nitrogen by carbon and M^{2+} by RE^{3+}. The silicon−nitride−carbide consists of a three-dimensional network of star-like $[C(SiN_3)_4]$ units, which are isoelectronic to the characteristic building $[N(SiN_3)_4]$ units in $MRESi_4N_7$ (M = Ba, Sr, Ca, Eu; RE = Y, Yb) compounds.[7−14] These units are connected by sharing $N^{[2]}$ (i.e., one nitrogen coordinates with two silicon, NSi_2) atoms to form two kinds of layers with diametrical orientation of the SiN_3C tetrahedrons. Along [001] these two types of layers are alternately connected by $N^{[2]}$ atoms to build up the three-dimensional condensed framework $[Si_4N_6C]^{6-}$. Similar to $MRESi_4N_7$ (M = Ba, Sr, Ca, Eu; RE = Y, Yb), the rare-earth ions are located at the channels along [100].[1,15] Because of the substitution of N^{3-} by C^{4-} in $MRESi_4N_7$, that is, the replacement of the fourfold coordinated nitrogen atoms by carbon in the framework, the lattice becomes more rigid due to the Si−C bond which has a higher degree of covalence than the Si−N bond. As a consequence, these compounds are interesting host lattices for phosphors due to their high mechanical hardness and their exceptional thermal and chemical stability.[1,15] However, to the best of our knowledge, no investigations have been performed on studying the luminescence properties of rare earth ions in these host lattices except for a few publications[5,6,16,17] focused on studying the luminescence properties of Ce^{3+} and Tb^{3+} in the $Y_2Si_4N_6C$ host lattice. In the present work, we report the luminescence properties of Ce^{3+} and Tb^{3+} singly doped and Tb^{3+}/ Ce^{3+}-codoped $RE_2Si_4N_6C$ (RE = Lu, Y, and Gd) phosphors, discuss the influence of the type of RE ion on the luminescence properties of these phosphors, and explore their

Received: December 8, 2010
Revised: March 1, 2011
Published: March 15, 2011

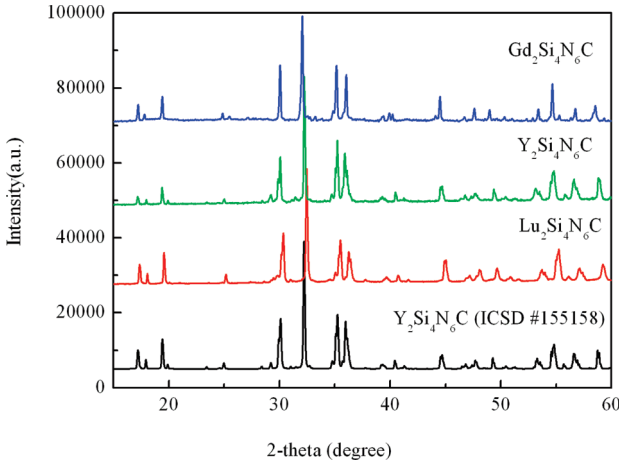

Figure 1. Powder XRD patterns of $RE_2Si_4N_6C$ (RE = Lu, Y, and Gd).

potential possibilities to be used as a new kind of LED phosphors. We also tried to investigate the luminescence properties of rare earth ions in the analogue compound of $La_2Si_4N_6C$ but failed to prepare the pure phase. Therefore, no information is given on the luminescence properties of rare earth ions in the $La_2Si_4N_6C$ host lattice in the present work.

2. EXPERIMENTAL SECTION

2.1. Synthesis of Undoped, Tb^{3+}-, Ce^{3+}-, and Ce^{3+}/Tb^{3+}-Doped $RE_2Si_4N_6C$ (RE = Lu, Y, and Gd). Polycrystalline undoped, Tb^{3+}-, Ce^{3+}-, and Ce^{3+}/Tb^{3+}-doped $RE_2Si_4N_6C$ (RE = Lu, Y, and Gd) powders were prepared by a high temperature solid-state reaction method. The stoichiometric amounts of rare earth metal powders Tb, Ce, Lu, Y, and Gd (Csre, >99%), SiC (Alfa, 99%), and α-Si_3N_4 (Permascand, P95H, measured α content 93%; oxygen content: ~1.5%) were weighed out and subsequently mixed and ground together in an agate mortar. All manipulations were performed in a dry glovebox flushed with dry nitrogen because some starting materials are air and moisture sensitive. The powder mixtures were then transferred into a closed molybdenum crucible. Subsequently, those powder mixtures were fired at 1650 °C for 10 h in a chamber furnace under a nitrogen atmosphere. After firing, the samples were gradually cooled down to room temperature in the furnace. There was no apparent reaction of the prepared materials with the Mo crucibles.

2.2. X-ray Diffraction Data Collection. The powder XRD data for phase identification were collected at ambient temperature by X-ray powder diffractometer (Bruker, D4 Endeavor X-ray Diffractometer) with Cu Kα radiation operated at 40 kV and 40 mA with a scan speed of 2°/min in the 2θ range of 10−90°. The powder XRD data for lattice parameters determination and structure refinement were collected at ambient temperature with a HUBER Imaging Plate Guinier Camera G670[S] (Cu Kα1 radiation, λ = 1.54056A°, Gemonochromator). The 2θ ranges are from 4 to 100° with a step of 0.005°. The FullProf program[18] was used to refine the structure.

2.3. Optical Measurements. The diffuse reflectance, emission, and excitation spectra of the samples were measured at room temperature in air by a Perkin-Elmer LS 50B spectrophotometer equipped with a Xe flash lamp. The reflection spectra were calibrated with the reflection of black felt (reflection 3%) and white barium sulfate ($BaSO_4$, reflection ~100%) in the wavelength region of 230−700 nm. The excitation and emission slits were set at 15 nm. The emission spectra were corrected by dividing the measured emission intensity by the ratio of the observed spectrum of a calibrated W-lamp and its known spectrum from 300 to 900 nm.

Table 1. Lattice Parameters of $RE_2Si_4N_6C$ (RE = Lu, Y, and Gd)

formula	$Lu_2Si_4N_6C$	$Y_2Si_4N_6C$	$Gd_2Si_4N_6C$
crystal system	monoclinic	monoclinic	monoclinic
space group	$P2_1/c$	$P2_1/c$	$P2_1/c$
lattice parameters			
a (Å)	5.8926 (2)	5.9295 (1)	5.9575 (2)
b (Å)	9.8605 (5)	9.8957 (1)	9.9957 (2)
c (Å)	11.8225 (3)	11.8800 (2)	11.9079(6)
β (deg)	120.17 (6)	119.63 (4)	119.91 (9)
V (Å^3)	593.85	605.92	614.61

Excitation spectra were automatically corrected for the variation in the lamp intensity by a second photomultiplier and a beam splitter. All the luminescence spectra were measured with a scan speed of 400 nm/min.

3. RESULTS AND DISCUSSION

3.1. Phase Formation. Figure 1 shows the typical powder XRD patterns of the $RE_2Si_4N_6C$ (RE = Lu, Y, and Gd) samples. The XRD patterns of $Y_2Si_4N_6C$ are in good agreement with those reported in ICSD no. 155158.[5] For $Lu_2Si_4N_6C$ and $Gd_2Si_4N_6C$, no similar structural data of these compounds are available for comparison. However, due to the similar ionic size of Lu^{3+} (0.861 Å), Y^{3+} (0.90 Å), and Gd^{3+} (0.938 Å),[19] it is reasonable to assume that a complete solid solution is very likely to form in the series of $RE_2Si_4N_6C$ (RE = Lu, Y, and Gd) compounds, which is indeed experimentally observed. As can be observed in Figure 1, when the Y^{3+} ions are substituted completely by Lu^{3+} or Gd^{3+} ions, the XRD patterns are almost the same except that there is a discernible shift in the position of the XRD peaks, which can be explained by the difference between the ionic radii of these rare-earth metals. With increasing the ionic radius of RE^{3+}, the XRD peaks of $RE_2Si_4N_6C$ shift to a lower 2-θ angle. We have also carried out an XRD cell parameters refinement based on the diffraction peaks obtained from the XRD patterns of $RE_2Si_4N_6C$ using the monoclinic crystal system established for $Y_2Si_4N_6C$,[5] and the results are summarized in Table 1. It is clear that the lattice parameters a, b, c, and V increase systematically with increasing rare-earth ionic radius [$r_{Lu^{3+}}$ (0.861 Å) < $r_{Y^{3+}}$ (0.90 Å) < $r_{Gd^{3+}}$ (0.938 Å)],[19] which also indicates that a complete solid solution is expected to form in the series of $RE_2Si_4N_6C$ (RE = Lu, Y, and Gd) compounds. Therefore, we can conclude that $RE_2Si_4N_6C$ (RE = Lu, Y, and Gd) compounds are isostructural.

In the crystal structure of $Y_2Si_4N_6C$,[6] there are two different crystallographic sites for the Y^{3+} ions. As shown in Figure 2, the Y(I) site is coordinated by five N atoms, while the Y(II) site is coordinated by six N atoms. The mean distance Y(I)−N (2.372 Å) is smaller than that of Y(II)−N (2.398 Å). The Y(II) site is larger than the Y(I) site because it possesses a larger coordination number together with a larger coordination polyhedron volume. Due to the quite similar ionic sizes of Lu^{3+} and Y^{3+} and the same XRD patterns of $Lu_2Si_4N_6C$ and $Y_2Si_4N_6C$, it is reasonable to assume that the coordination environments of Lu^{3+} in $Lu_2Si_4N_6C$ are similar to those of Y^{3+} in $Y_2Si_4N_6C$. On the contrary, the exact coordination environments of Gd^{3+} in $Gd_2Si_4N_6C$ are difficult to predict due to the rather large size difference between Gd^{3+} and RE^{3+} (RE = Lu, Y). As a consequence, a Rietveld analysis was performed to get more detailed

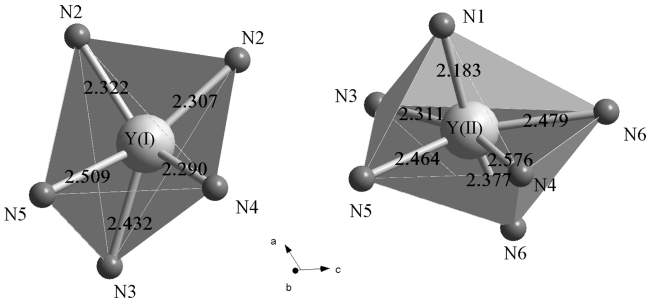

Figure 2. Nitrogen atom coordination of the two different Y^{3+} sites in $Y_2Si_4N_6C$.

Table 2. Structural Parameters for $Gd_2Si_4N_6C$ As Determined by Rietveld Refinement of Powder XRD Data at Room Temperature[a]

atom	Wyck.	*x*	*y*	*z*	*U* (Å^2)
Gd1	4*e*	0.3326(7)	0.5672(7)	0.0950(3)	0.0101
Gd2	4*e*	0.6710(8)	0.4183(6)	0.4184(4)	0.0086
Si1	4*e*	0.0050(7)	0.4804(5)	0.2498(8)	0.0077
Si2	4*e*	0.1640(8)	0.2132(8)	0.4217(8)	0.0076
Si3	4*e*	0.2018(2)	0.2059(8)	0.1763(7)	0.0080
Si4	4*e*	0.6767(2)	0.2281(9)	0.1590(8)	0.0080
N1	4*e*	0.0430(5)	0.2110(7)	0.0089(9)	0.0145
N2	4*e*	0.0590(3)	0.0456(8)	0.3995(7)	0.0093
N3	4*e*	0.2410(3)	0.0356(8)	0.2234(7)	0.0099
N4	4*e*	0.5070(4)	0.2910(8)	0.0016(2)	0.0115
N5	4*e*	0.5170(4)	0.2646(5)	0.2452(5)	0.0111
N6	4*e*	0.6990(3)	0.0532(9)	0.1373(6)	0.0095
C1	4*e*	0.0220(6)	0.2916(5)	0.2519(8)	0.0076

[a] Space group: $P2_1/c$ (No. 14), $Z = 4$, $a = 5.9575(2)$ Å, $b = 9.9957(2)$ Å, $c = 11.9079(5)$ Å, $\beta = 119.92(0)°$, $V = 614.61$ Å^3, *R*p = 33.4%, *R*wp = 14.7%, *R*exp = 25.50%.

information about it. Here the atom coordination of $Ho_2Si_4N_6C$[1] with space group $P2_1/c$ was used as starting parameters for the refinement of $Gd_2Si_4N_6C$. According to the original structure model described above, we refined the structure parameters of $Gd_2Si_4N_6C$ with the powder X-ray diffraction data by the Rietveld method using the FullProf program.[18] The final *R* factors, the refined lattice constants, and atomic and thermal parameters for $Gd_2Si_4N_6C$ are shown in Table 2. Figure 3 shows the Rietveld refinement results for $Gd_2Si_4N_6C$. The red lines represent the observed diffraction patterns, the black lines represent the calculated diffraction patterns, and the blue curves at the bottom of the figure represent the difference. The short vertical green lines mark the positions of possible Bragg reflections for $Gd_2Si_4N_6C$. The remarkably good fit between the observed and calculated patterns supports the structure parameters listed in Table 2. Figure 3 shows the coordination environments of Gd^{3+} in $Gd_2Si_4N_6C$. There are also two different crystallographic sites for the Gd^{3+} ions. As shown in Figure 4, the Gd(I) site is coordinated by five N atoms, while the Gd(II) site is coordinated by six N atoms. The mean distance Gd(I)−N (2.403 Å) is smaller than that of Gd(II)−N (2.436 Å). The Gd(II) site is larger than the Gd(I) site.

3.2. Luminescence Properties of Tb^{3+}-Doped Materials. The luminescence properties of Tb^{3+} ions in $RE_2Si_4N_6C$ (RE = Lu, Y, and Gd) host lattices are similar (Figures 5−7). $RE_2Si_4N_6C$:Tb^{3+} (20 mol %) phosphors exhibit a group of typical sharp emission lines in the wavelength range of 470−650 nm corresponding to the $^5D_4 \rightarrow {}^7F_J$ (J = 6, 5, 4, 3) transitions of Tb^{3+} under UV excitation around 300 nm. The dominant one is the $^5D_4 \rightarrow {}^7F_5$ transition at about 548 nm. The blue emissions at wavelengths below 489 nm originating from the $^5D_3 \rightarrow {}^7F_J$ transitions of Tb^{3+} ions have not been observed. This can be explained by the well-known cross-relaxation between the $^5D_3$ and $^5D_4$ of Tb^{3+} at a higher Tb^{3+} doping concentration.[20−22] The excitation spectra consist of a strong band in the wavelength range of 250−350 nm with peak centers at about 300 nm for RE = Lu and Y and 320 nm for RE = Gd and in addition some very weak sharp lines in the wavelength range of 350−500 nm (Figures 5−7). For Tb^{3+} ions with $4f^8$ electrons configuration, the ground states are $^7F_6$. When one electron is promoted to the 5d shell, it gives rise to two $4f^7$5d excitation states: the high-spin state with ^9D_J configurations or low-spin state with ^7D_J configurations. Obviously, ^9D_J states will be lower in energy according to the Hund's rule, and the transitions between $^7F_6$ and ^7D_J are spin-allowed, while the transitions between $^7F_6$ and ^9D_J are spin-forbidden. Therefore, Tb^{3+} in a specific host lattice usually exhibits two groups of 4f → 5d transitions: The spin-allowed 4f → 5d transitions are strong and at higher energy while the spin-forbidden 4f → 5d transitions are weak and at lower energy. Therefore, the strong excitation band observed around 300−320 nm in the excitation spectra of Tb^{3+}-doped $RE_2Si_4N_6C$ phosphors can be ascribed to the lowest spin-allowed 4f → 5d transition of Tb^{3+} in these host lattices while the spin-forbidden 4f → 5d transition of Tb^{3+} at longer wavelengths is too weak to be observed. Some weak sharp lines at low energy (i.e., from 350 to 500 nm) can be ascribed to the transition between the energy levels within the $4f^8$ configuration, that is, $^7F_6 \rightarrow {}^5D_3$ and $^7F_6 \rightarrow {}^5D_4$. For the purpose of clarity, the intensity of them is magnified as much as five times.

The emission intensities of $(RE_{1-x}Tb_x)_2Si_4N_6C$ ($0.01 \le x \le 0.5$) phosphors as a function of the Tb^{3+} concentration under excitation wavelength of 300 nm are presented in Figure 8. For all Tb^{3+}-doped $RE_2Si_4N_6C$ (RE = Lu, Y, and Gd) phosphors, the optimal emission intensity is observed for the material doped with 20 mol % Tb^{3+} (i.e., x = 0.20). The emission intensity declines intensively as the concentration of Tb^{3+} exceeds 20 mol % due to concentration quenching, more or less in the same way for the different phosphors.

Table 3 summarizes the characteristics of $RE_2Si_4N_6C$:Tb^{3+} (20 mol %) (RE = Lu, Y, and Gd) phosphors and compares them with some other typical Tb^{3+}-doped phosphors. From the comparison, we can see that there is no great change for the position of the dominant line emission of Tb^{3+} in different kinds of host lattices. However, there is a great change for the position of the 4f → 5d (spin-allowed) excitation bands of the Tb^{3+} ion. Normally, Tb^{3+}-doped phosphors show a broad excitation band in the wavelength range of 200−300 nm originating from the spin-allowed 4f → 5d transition of Tb^{3+},[23] such as YF_3:Tb^{3+},[24] YOF:Tb^{3+},[25] Y_2O_3:Tb^{3+},[26] Y_2O_2S:Tb^{3+},[27] Ba_7SiN_{10}:Tb^{3+},[28] $LiSi_2N_3$:Tb^{3+},[29] and so forth. So a similar excitation band would be expected for Tb^{3+} in $RE_2Si_4N_6C$ host lattice. However, this is not the case. The 5d excitation bands of Tb^{3+} in $RE_2Si_4N_6C$ (RE = Lu, Y, and Gd) host lattices are located at a longer wavelength range, which is rather particular. It can be explained by a highly covalent host lattice due to the presence of N as well as C in the silicon−nitride−carbide network. Thus, Tb^{3+}- activated

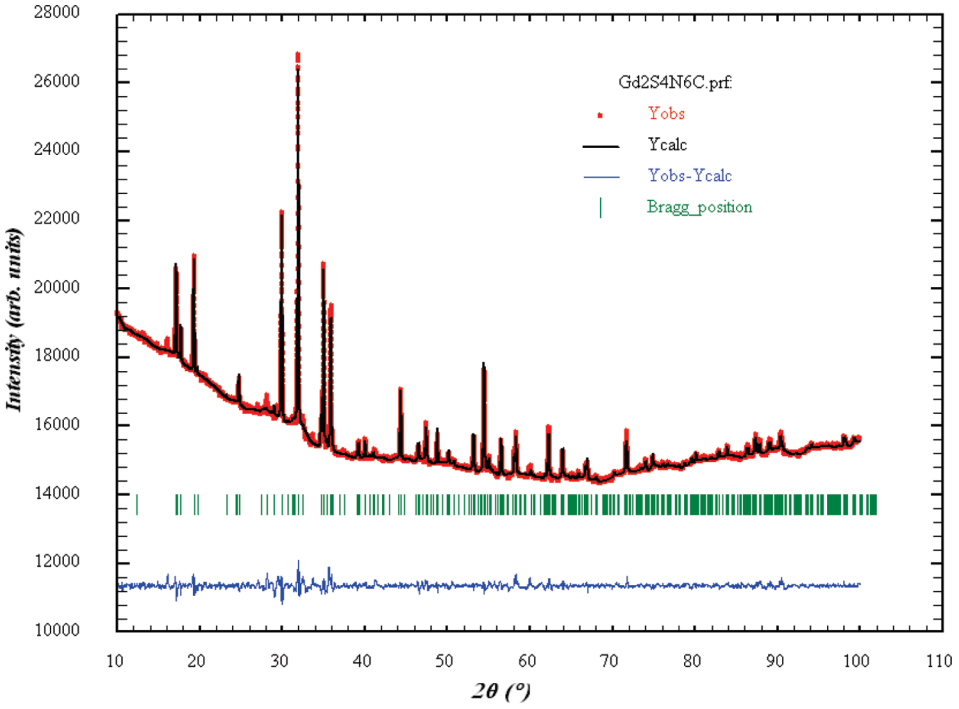

Figure 3. Observed (red) and calculated (black) X-ray powder diffraction patterns and the difference profile (blue) of the Rietveld refinement of $Gd_2Si_4N_6C$.

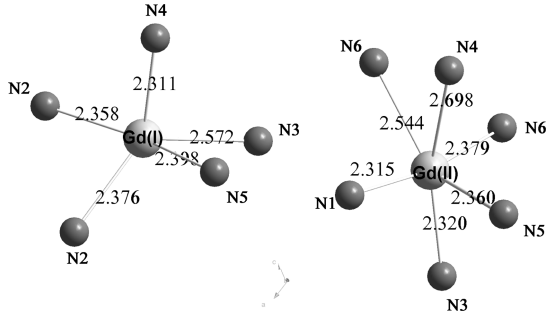

Figure 4. Nitrogen atom coordination of the two different Gd^{3+} sites in $Gd_2Si_4N_6C$.

$RE_2Si_4N_6C$ (RE = Lu, Y, and Gd) phosphors can be efficiently excited at a rather long wavelength, which makes them interesting line green-emitting phosphors for UV light-emitting diodes applications.

3.3. Luminescence Properties of Ce^{3+}-Doped Materials. The luminescence properties of Ce^{3+} ions in $Lu_2Si_4N_6C$ and $Y_2Si_4N_6C$ host lattices are very similar (Figures 9 and 10). Both Ce^{3+}-activated $Lu_2Si_4N_6C$ and $Y_2Si_4N_6C$ phosphors exhibit a broad emission band in the wavelength range of 450−700 nm with peak centers at about 540 and 535 nm for RE = Lu and Y, respectively. Obviously, the observed band emission can be ascribed to the transition from the lowest energy crystal field splitting component of the 5d level to the 4f ground state of Ce^{3+} incorporated in the $RE_2Si_4N_6C$ host lattice. By varying the excitation wavelength the same emission band was found implying that there is only one Ce^{3+} luminescent center in $RE_2Si_4N_6C:Ce^{3+}$ (1 mol %) (RE = Lu, Y) phosphors. In the crystal structure of $RE_2Si_4N_6C$ (RE = Lu, Y) (Section 3.1), there are two

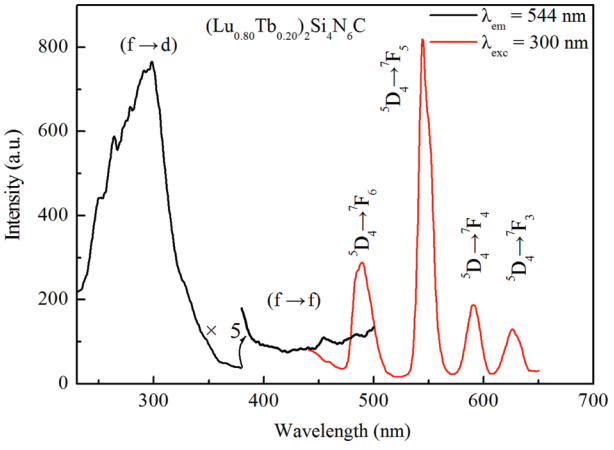

Figure 5. Typical excitation and emission spectra of Tb^{3+}-doped $Lu_2Si_4N_6C$ phosphor.

different crystallographic sites for the RE^{3+} ions. One possible explanation for the appearance of the single Ce^{3+} luminescent center in $RE_2Si_4N_6C:Ce^{3+}$ (1 mol %) phosphor is that only one RE^{3+} site is occupied by the dopant Ce^{3+} ion due to the large size difference between Ce^{3+} and RE^{3+} ions [$(r_{RE^{3+}} < r_{Ce^{3+}})$ (RE = Lu, Y)]. The larger dopant Ce^{3+} ion may prefer to substitute the larger RE(II) site in $RE_2Si_4N_6C$ host lattice because of best matching of ion sizes. On an energy scale, the emission band can be decomposed into two well-separated Gaussian components with peak centers at about 17514 and 19570 cm^{-1} (corresponding to 571 and 511 nm, respectively) for $Lu_2Si_4N_6C:Ce^{3+}$ (1 mol %) and 17595 and 19407 cm^{-1} (corresponding to 568 and 515 nm, respectively) for $Y_2Si_4N_6C:Ce^{3+}$ (1 mol %) (as shown in Figures 11 and 12).

dx.doi.org/10.1021/cm103495j |*Chem. Mater.* 2011, 23, 1851–1861

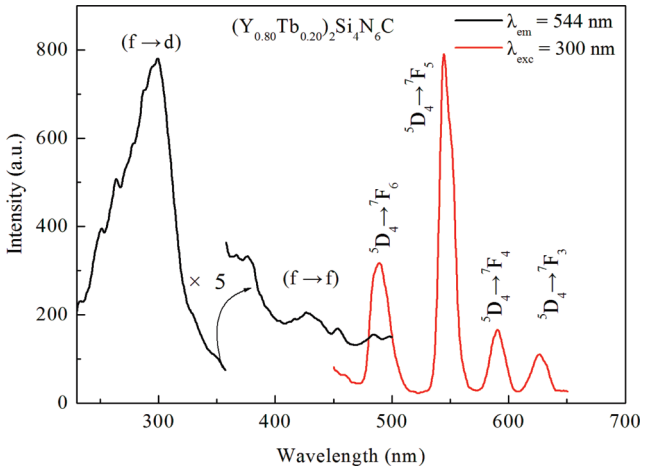

Figure 6. Typical excitation and emission spectra of Tb^{3+}-doped $Y_2Si_4N_6C$ phosphor.

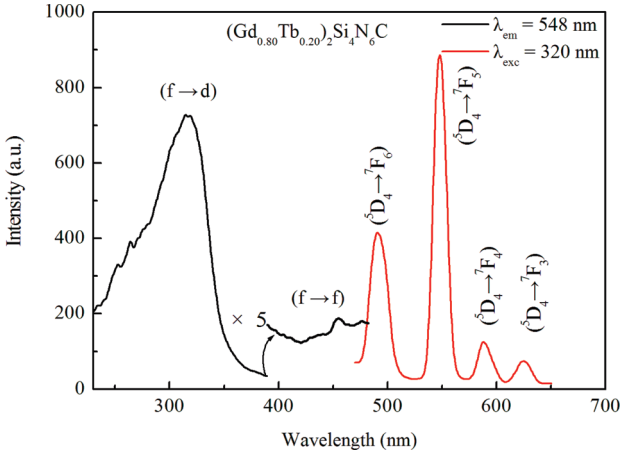

Figure 7. Typical excitation and emission spectra of Tb^{3+}-doped $Gd_2Si_4N_6C$ phosphor.

As indicated above, there is only one Ce^{3+} luminescent center in $RE_2Si_4N_6C:Ce^{3+}$ (1 mol %) phosphor, so the two separated Gaussian components can be attributed to the emission from the lowest 5d level to the $^2F_{5/2}(4f^1)$ and $^2F_{7/2}(4f^1)$ ground state levels of Ce^{3+} incorporated in the $RE_2Si_4N_6C$ host lattice. The energy differences between the two Gaussian components are 1812 and 2100 cm^{-1} for $Y_2Si_4N_6C:Ce^{3+}$ (1 mol %) and $Lu_2Si_4N_6C:Ce^{3+}$ (1 mol %), respectively, which is close to the energy difference normally observed between the $^2F_{5/2}$ and $^2F_{7/2}$ ground state levels of Ce^{3+} [$(\Delta(^2F_{5/2}-{}^2F_{7/2}) \approx 2000-2200\ cm^{-1}$].[30] The excitation spectra of Ce^{3+}-activated $RE_2Si_4N_6C$ (RE = Lu, Y) phosphors show three bands with peak centers at about 261, 385, and 428 nm for RE = Lu and 280, 387, and 426 nm for RE = Y. (Figures 9 and 10). Definitely, the short weak excitation bands below 300 nm can be ascribed to the host lattice excitation as can be concluded from the comparison with the reflection spectra of undoped $Lu_2Si_4N_6C$ and $Y_2Si_4N_6C$ samples (see Supporting Information, Figure S1). The appearance of the host lattice excitation bands in the excitation spectrum of Ce^{3+} indicates that there exists energy transfer from the $RE_2Si_4N_6C$ host lattice to Ce^{3+}. The remaining two strong excitation bands in the wavelength range of 350−500 nm can be assigned to the Ce^{3+} transition from the 4f ground state to the 5d levels splitted by the crystal field.

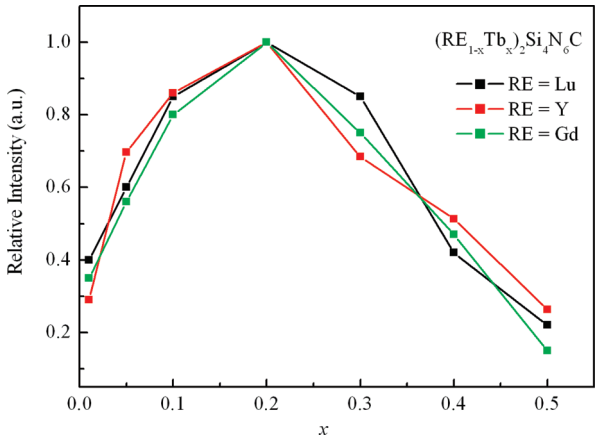

Figure 8. Emission intensities of $(RE_{1-x}Tb_x)_2Si_4N_6C$ under excitation wavelength of 300 nm as a function of the Tb concentration.

The luminescence properties of Ce^{3+} ions in $Gd_2Si_4N_6C$ are different from those of Ce^{3+} ions in $Lu_2Si_4N_6C$ and $Y_2Si_4N_6C$ host lattices (Figure 13) although $RE_2Si_4N_6C$ (RE = Lu, Y, and Gd) are isostructural compounds. Ce^{3+}-activated $Gd_2Si_4N_6C$ shows a very broad emission band in the wavelength range of 500−800 nm. By changing the excitation wavelength from 400 to 490 nm, the peak center of this emission band shifted from 595 to 610 nm. In addition, no luminescence has been found for undoped $Gd_2Si_4N_6C$ sample. These facts indicate that there are two different Ce^{3+} luminescent centers in $Gd_2Si_4N_6C:Ce^{3+}$ (1 mol %) phosphor. However, by varying the excitation wavelength from 465 to 490 nm, the same Ce^{3+} emission band was found. It shows a broad emission band in the wavelength range of 500−800 nm with peak center at about 610 nm. Therefore, we can reasonably assign this emission band to a single Ce^{3+} luminescent center (i.e., the first Ce^{3+} luminescent center) in the $Gd_2Si_4N_6C:Ce^{3+}$ (1 mol %) phosphor. On an energy scale, this emission band can be decomposed into two well-separated Gaussian components with peak centers at about 15250 and 17230 cm^{-1} (corresponding to 656 and 580 nm, respectively) (as shown in Figure 14), which can be attributed to the transition from the lowest 5d level to the $^2F_{5/2}$ and $^2F_{7/2}$ levels of Ce^{3+} in $Gd_2Si_4N_6C$ host lattice. The energy difference between them is 1980 cm^{-1}, which is in good agreement with the generally observed energy difference between the $^2F_{5/2}$ and $^2F_{7/2}$ ground state levels of Ce^{3+} [$\Delta(^2F_{5/2} - {}^2F_{7/2}) \approx 2000-2200\ cm^{-1}$]. By varying the excitation wavelength from 350 to 425 nm, besides the strong emission band from the first Ce^{3+} luminescent center a weak shoulder emission band in the short wavelength range can also be observed, which can be ascribed to the second Ce^{3+} luminescent center in $Gd_2Si_4N_6C:Ce^{3+}$ (1 mol %) phosphor. As shown in Figure 15, the emission band of Ce^{3+}-doped $Gd_2Si_4N_6C$ phosphor under excitation of 425 nm can be decomposed into three Gaussian components with peak centers at about 15300, 17200, and 18760 cm^{-1} (corresponding to 654, 581, and 533 nm, respectively) on an energy scale. The former two Gaussian components (peaking at 654 and 581 nm) and the third weak one (peaking at about 533 nm) can be assigned to the emission from the first and the second Ce^{3+} luminescent center in $Gd_2Si_4N_6C$ phosphor, respectively. In the crystal structure of $Gd_2Si_4N_6C$, there are also two different crystallographic sites for

dx.doi.org/10.1021/cm103495j |Chem. Mater. 2011, 23, 1851–1861

Table 3. Characteristics of Tb^{3+}-Doped $RE_2Si_4N_6C$ (RE = Lu, Y, and Gd) Phosphors As Compared to Those of Typical Tb^{3+}-Doped Phosphors at Room Temperature

phosphors	$Lu_2Si_4N_6C$: Tb^{3+}	$Y_2Si_4N_6C$: Tb^{3+}	$Gd_2Si_4N_6C$: Tb^{3+}	YF_3: Tb^{3+}	YOF: Tb^{3+}	Y_2O_3: Tb^{3+}	Y_2O_2S:Tb^{3+} (high concentration)	Ba_7SiN_{10}: Tb^{3+}	$LiSi_2N_3$: Tb^{3+}
crystal system	$P2_1/c$	$P2_1/c$	$P2_1/c$	*Pnma*	$R\bar{3}mR$	$Ia\bar{3}$	$P\bar{3}m1$	*P*1*c*1	*Cmc*21
body color	gray	gray	gray	white	white	white	white	white	white
Tb^{3+} 5d excitation band maximum (nm)	300	300	320	213	<244	280	282	260	236
Tb^{3+} line emission maximum (nm)	544	544	548	545	545	545	544	546	542
ref	this work	this work,5 and 6	this work	24	25	26	27	28	29

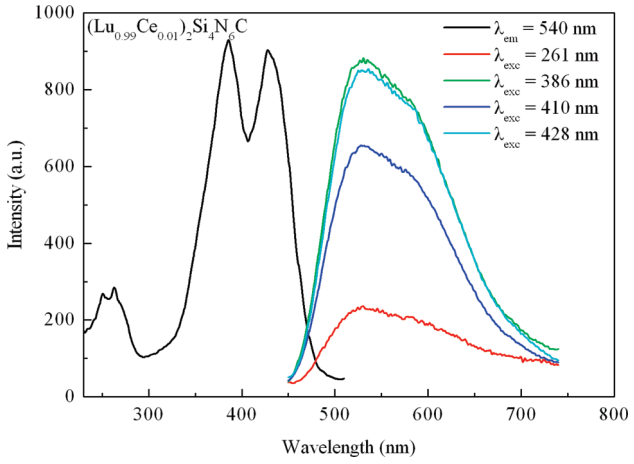

Figure 9. Typical excitation and emission spectra of Ce^{3+}-doped $Lu_2Si_4N_6C$ phosphor.

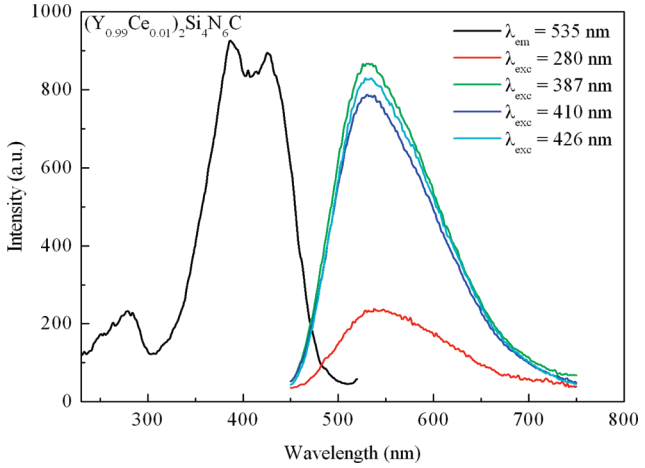

Figure 10. Typical excitation and emission spectra of Ce^{3+}-doped $Y_2Si_4N_6C$ phosphor.

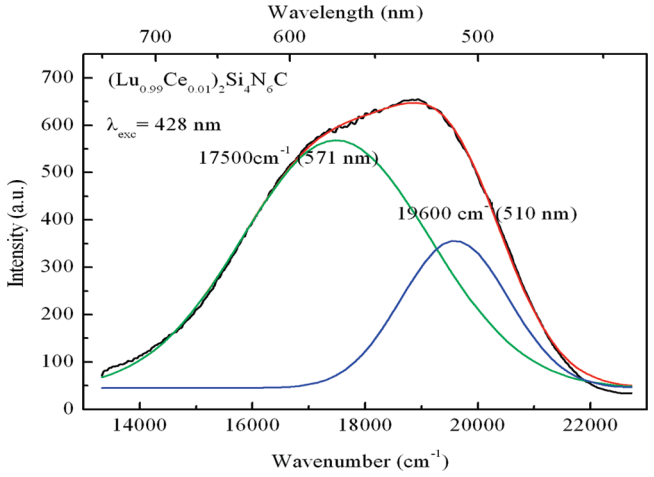

Figure 11. Deconvoluted emission spectrum of $(Lu_{0.99}Ce_{0.01})_2Si_4N_6C$ as a sum of two Gaussian bands.

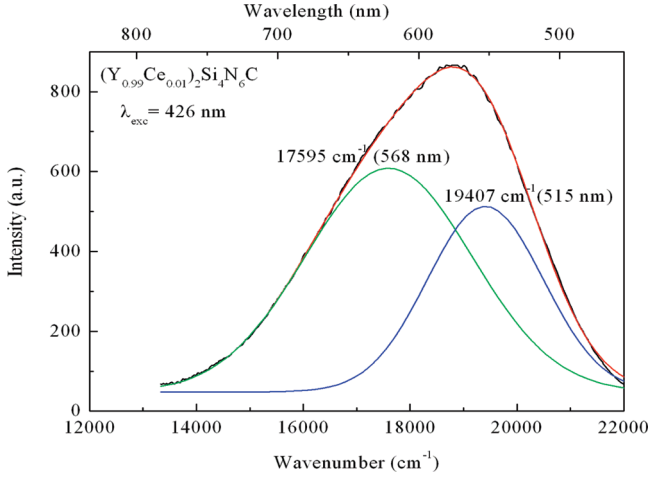

Figure 12. Deconvoluted emission spectrum of $(Y_{0.99}Ce_{0.01})_2Si_4N_6C$ as a sum of two Gaussian bands.

Gd^{3+} ions. Among the two sites, Gd(I) is smaller than the Gd(II) site (Section 3.1). As a consequence, the Ce^{3+} ions substituting the smaller Gd(I) site experience a stronger crystal field strength, which is inversely proportional to R^5 (R: chemical bond length between a cation with d ortital electrons and the coordinating anion),[31] resulting in a longer wavelength emission. Therefore, we can reasonably assign the longer wavelength emission band with peak center at about 610 nm to the Ce^{3+} ions substituting at the Gd(I) site (i.e., $Ce_{Gd(I)}$) and the weak shoulder emission band in the short wavelength range at about 533 nm to Ce^{3+} ions substituting at the Gd(II) site (i.e., $Ce_{Gd(II)}$). Because the size of Ce^{3+} is larger than that of Gd^{3+}, it is reasonable to assume that the dopant Ce^{3+} ion may prefer to occupy the larger Gd(II) site. As a consequence in first glance, a dominant emission from $Ce_{Gd(II)}$ would be expected. However, this is not the case. One possible explanation for this phenomenon is that there exists efficient energy transfer from $Ce_{Gd(II)}$ to $Ce_{Gd(I)}$. The $Ce_{Gd(II)}$ center transfers most of its absorbed energy to the nearest

dx.doi.org/10.1021/cm103495j |*Chem. Mater.* 2011, 23, 1851–1861

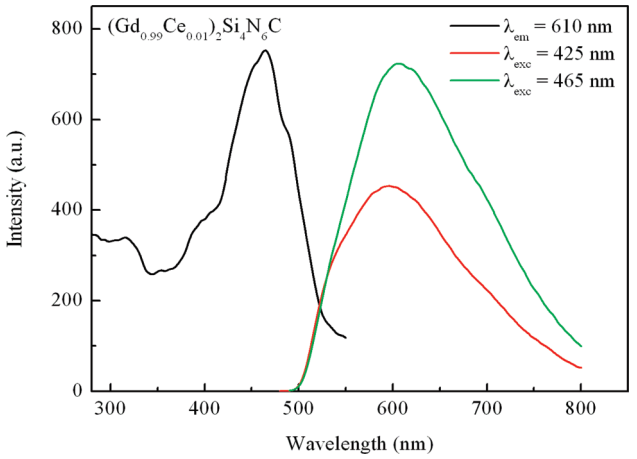

Figure 13. Typical excitation and emission spectra of Ce^{3+}-doped $Gd_2Si_4N_6C$ phosphor.

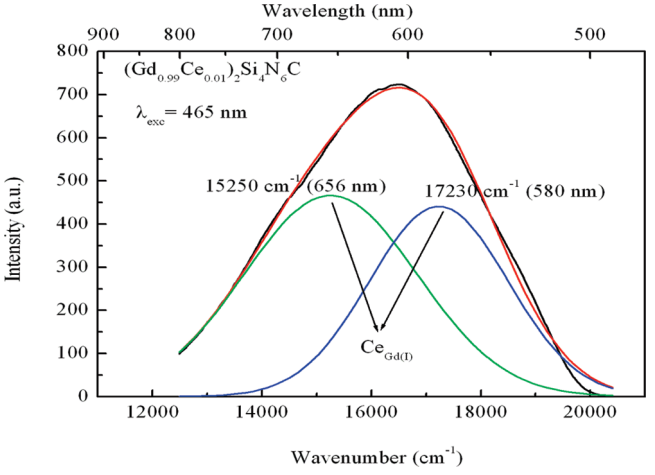

Figure 14. Deconvoluted emission spectrum of $(Gd_{0.99}Ce_{0.01})_2Si_4N_6C$ as a sum of two Gaussian bands.

neighbor $Ce_{Gd(I)}$ center and results in the dominant emission from the $Ce_{Gd(I)}$ center. The exact explanation is the subject of further study. By monitoring the emission peak at 610 nm ($Ce_{Gd(I)}$ center), the excitation spectrum of Ce^{3+}-doped $Gd_2Si_4N_6C$ show two bands with peak centers at about 310 and 465 nm. Definitely, the short weak excitation band below 350 nm can be ascribed to the host lattice excitation as can be concluded from the comparison with the reflection spectrum of undoped $Gd_2Si_4N_6C$ sample (see Supporting Information, Figure S1). The appearance of the host lattice excitation bands in the excitation spectrum of Ce^{3+} indicates that there exists energy transfer from the $Gd_2Si_4N_6C$ host lattice to Ce^{3+}. The remaining strong excitation band in the wavelength range of 400−550 nm can be assigned to the transition from the 4f ground state to the 5d levels splitted by crystal field of the excited Ce^{3+} ions substituting at the Gd(I) site. Due to the strong overlap between the two emission bands of Ce^{3+} ion, the excitation spectrum of Ce^{3+}-doped $Gd_2Si_4N_6C$ does not show great change by changing the monitoring wavelengths from 610 ($Ce_{Gd(I)}$ center) to 533 nm ($Ce_{Gd(II)}$ center).

The excitation and emission bands of Ce^{3+} in $RE_2Si_4N_6C$ (RE = Lu, Y, and Gd) host lattices are located at a longer wavelength

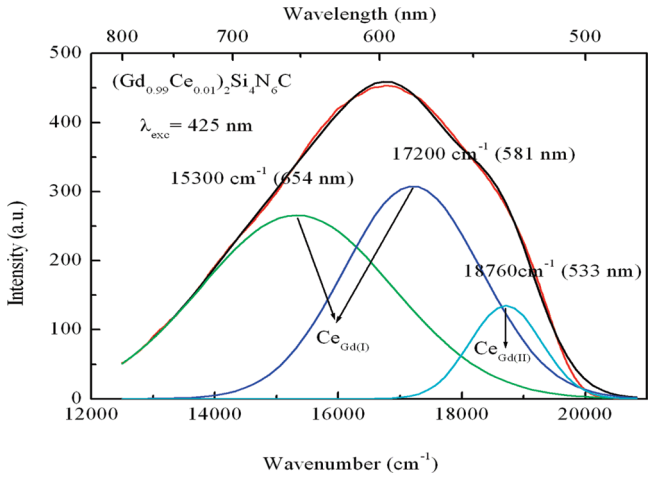

Figure 15. Deconvoluted emission spectrum of $(Gd_{0.99}Ce_{0.01})_2Si_4N_6C$ as a sum of three Gaussian bands.

range than usually observed, which mainly can be ascribed to the effect of a high covalency and a large crystal field splitting on the 5d band of Ce^{3+} in the nitrogen coordination environment. Similar phenomena have been found in some other Ce^{3+}-doped nitride phosphors, such as Ce^{3+}-doped $M_2Si_5N_8$ (M = Ca, Sr, and Ba),[32] $MSiN_2$ (M = Ca, Sr, and Ba),[33,34] and $CaAlSiN_3$[35] phosphors, etc. Of course, the effect of carbon atoms on increasing the covalency of the silicon−nitride−carbide network also cannot be ignored.

Here, it is worth noting that Ce^{3+}-doped $RE_2Si_4N_6C$ (RE = Lu, Y, and Gd) phosphors can be efficiently excited in the wavelength range of 350−500, which perfectly matches with the radiative light from the InGaN- or GaN-based LEDs. Thus, the luminescence properties of $RE_2Si_4N_6C$:Ce^{3+} phosphors are favorable for white LED applications.

Table 4 summarizes the composition, phase characteristics, and luminescence properties of Ce^{3+}-doped $RE_2Si_4N_6C$ (RE = Lu, Y, and Gd) for a comparison. For the isostructural $RE_2Si_4N_6C$ (RE = Lu, Y, and Gd) compounds, the luminescence properties of Ce^{3+} ions in these host lattices are influenced by the size of RE^{3+} ions ($Lu_2Si_4N_6C$ and $Y_2Si_4N_6C$ vs $Gd_2Si_4N_6C$). There is only one Ce^{3+} luminescent center [i.e.$Ce_{RE(II)}$] in Ce^{3+}-doped $RE_2Si_4N_6C$ (RE = Lu, Y) phosphors, while there are two different Ce^{3+} luminescent centers [i.e., $Ce_{Gd(I)}$ and $Ce_{Gd(II)}$] in Ce^{3+}-doped $Gd_2Si_4N_6C$ phosphor. This difference can be ascribed to the size difference between Ce^{3+}, Gd^{3+}, Y^{3+}, and Lu^{3+} ions. The sequence of the sizes of these rare earth ions is $Ce^{3+} > Gd^{3+} > Y^{3+} > Lu^{3+}$.[19] The Gd^{3+} ion is larger than Lu^{3+} and Y^{3+} ions but smaller than the Ce^{3+} ion. In other words, it also means that the size of the Gd^{3+} ion is more close to that of the larger dopant Ce^{3+} ion than those of the smaller Lu^{3+} and Y^{3+} ions. As a consequence, even at a low doping concentration, Ce^{3+} ions still prefer to occupy the two different Gd(I) and Gd(II) sites simultaneously in Ce^{3+}-doped $Gd_2Si_4N_6C$ phosphor instead of just only the single larger RE(II) site in Ce^{3+}-doped $RE_2Si_4N_6C$ (RE = Lu, Y) phosphors. This fact leads to similar luminescence properties for Ce^{3+} in $Lu_2Si_4N_6C$ and $Y_2Si_4N_6C$ host lattices but different ones for Ce^{3+} in the $Gd_2Si_4N_6C$ host lattice. In Ce^{3+}-doped $RE_2Si_4N_6C$ (RE = Lu, Y, and Gd) phosphors, the dominant emission is from the $Ce_{RE(I)}$ and $Ce_{RE(II)}$ centers for RE = Gd versus RE = Lu and Y, respectively.

dx.doi.org/10.1021/cm103495j |*Chem. Mater.* 2011, 23, 1851–1861

Table 4. Composition, Phase Characteristics, and Photoluminescence Properties of Ce^{3+}-Doped $RE_2Si_4N_6C$ (RE = Lu, Y, and Gd) Phosphors at Room Temperature

$RE_2Si_4N_6C:Ce^{3+}$ (1 mol %)	Lu[a]	Y[a]	Gd[a]
phase	$Lu_2Si_4N_6C$	$Y_2Si_4N_6C$	$Gd_2Si_4N_6C$
body color	green	green	peach-yellow
the number of Ce^{3+} luminescent centers	1 [$Ce_{Lu(II)}$]	1 [$Ce_{Y(II)}$]	2 {[$Ce_{Gd(I)}$], [$Ce_{Gd(II)}$]}
host lattice excitation bands (nm)	260	280	310
Ce 5d excitation bands (nm)	385, 428	387, 426	465 [$Ce_{Gd(I)}$]
emission band maximum (nm)	540	535	533 (weak), 610 (strong)
Stokes shift (cm^{-1})	~4850	~4670	~5100 [$Ce_{Gd(I)}$]
ref	this work	this work,5 and 6	this work

[a] RE = Lu < Y < Gd.

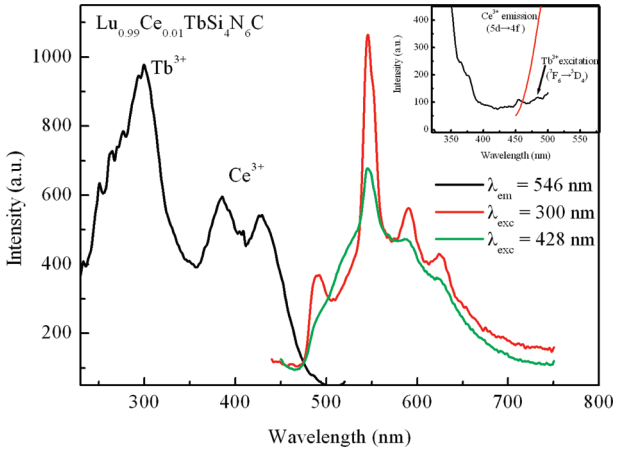

Figure 16. Typical excitation and emission spectra of Ce^{3+}/Tb^{3+}-codoped $Lu_2Si_4N_6C$ phosphor. Inset shows the partial overlap between the Ce^{3+} emission band and the $^5D_4$ excitation energy level of Tb^{3+} in $Lu_2Si_4N_6C$ host lattice.

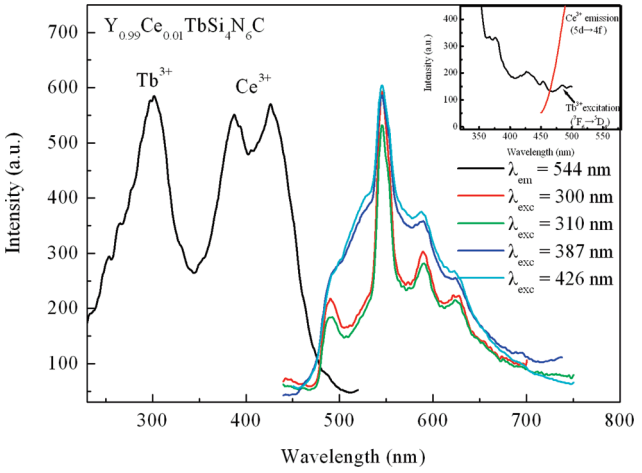

Figure 17. Typical excitation and emission spectra of Ce^{3+}/Tb^{3+}-codoped $Y_2Si_4N_6C$ phosphor. Inset shows the partial overlap between the Ce^{3+} emission band and the $^5D_4$ excitation energy level of Tb^{3+} in $Y_2Si_4N_6C$ host lattice.

3.4. Luminescence Properties of Ce^{3+}/Tb^{3+}-Codoped Materials. Codoping of Tb^{3+}-activated phosphors with Ce^{3+} acting as the sensitizer is well established for mercury gas-discharge lamps, for example, $CeMgAl_{10}O_{19}:Tb^{3+}$, $GdMgB_5O_{10}:Ce^{3+}$, Tb^{3+}, $LaPO_4:Ce^{3+},Tb^{3+}$.[30,36−38] For efficient energy transfer, a high concentration Tb^{3+} is usually required for quenching of the Ce^{3+} 5d → 4f and Tb^{3+} $^5D_3 \rightarrow {}^7F_J$ (i.e., due to the cross-relaxation process) emissions, respectively. In addition, an appropriate Ce^{3+} concentration (i.e., 1−3 mol %) is also helpful for quenching of the Ce^{3+} emission by energy migration.[6] Therefore, a series of samples codoped with a high concentration of Tb^{3+} (i.e., 50 mol %) and a low concentration of Ce^{3+} (i.e., 1 mol %) were prepared, that is, $RE_{0.99}Ce_{0.01}TbSi_4N_6C$ (RE = Lu, Y, and Gd). Because $Tb_2Si_4N_6C$ is isostructural with $RE_2Si_4N_6C$ (RE = Lu, Y, and Gd) compounds,[6] the crystal structure of the $RE_2Si_4N_6C$ host lattice does not show any change with the incorporation of a large amount of Tb^{3+} ions.

3.4.1. Energy Transfer from Ce^{3+} to Tb^{3+} in Ce^{3+}/Tb^{3+}-Codoped $Lu_2Si_4N_6C$ and $Y_2Si_4N_6C$ Phosphors. The luminescence properties of Ce^{3+}/Tb^{3+}-codoped $RE_2Si_4N_6C$ (RE = Lu, Y) phosphors are very similar (Figures 16 and 17). The excitation spectra of them show two main bands with the maxima at about 300 nm, and a second band composed of two sub-bands centered at 385 and 428 nm for RE = Lu versus 387 and 426 nm for RE = Y. By comparing them with the excitation spectra of the Tb^{3+} and Ce^{3+} singly doped $RE_2Si_4N_6C$ (RE = Lu, Y) phosphors, we can conclude that the first excitation band belongs to the spin allowed 4f → 5d transition of Tb^{3+} and the longer wavelength bands originate from the 4f → 5d transition of Ce^{3+} in these host lattices. Under the excitation of Ce^{3+} below 350 nm (i.e., from 280 to 350 nm), the emission spectrum mainly consists of a strong Tb^{3+} line emission together with a very weak Ce^{3+} band emission because the Tb^{3+} ions are be directly excited themselves via $^7F_6 \rightarrow$ 5d transition in this range. On the contrary, under the excitation of Ce^{3+} above 380 nm (i.e., from 390 to 470 nm) both Ce^{3+} band and Tb^{3+} line emission can be observed in the emission spectrum (Figures 16 and 17). On the basis of the fact that hardly any Tb^{3+} line emission ($^5D_4 \rightarrow {}^7F_J$, J = 6, 5, 4, 3, 2) can be observed with excitation wavelengths above 420 nm in the Tb^{3+} singly doped $Lu_2Si_4N_6C$ and $Y_2Si_4N_6$ phosphors, we can conclude that there exists energy transfer from Ce^{3+} to Tb^{3+} in Ce^{3+}/Tb^{3+}-codoped $RE_2Si_4N_6C$ (RE = Lu, Y) phosphors under the direct excitation of Ce^{3+} in the wavelength range of 380−470 nm. In the Ce^{3+} and Tb^{3+} singly doped $RE_2Si_4N_6C$ (RE = Lu, Y) phosphors, the Ce^{3+} emission band is overlapping with the $^7F_6 \rightarrow {}^5D_4$ excitation transition of Tb^{3+} (as shown in the inset of Figures 16 and 17), which results in energy transfer directly from the Ce^{3+} 5d band to the $^5D_4$ energy level of Tb^{3+} in Ce^{3+}/Tb^{3+}-codoped $RE_2Si_4N_6C$ phosphors. As a schematic diagram shown in Figure 18, the primary 5d excitation levels of Ce^{3+} are just situated between $^5D_3$ and $^5D_4$ energy levels

dx.doi.org/10.1021/cm103495j |Chem. Mater. 2011, 23, 1851–1861

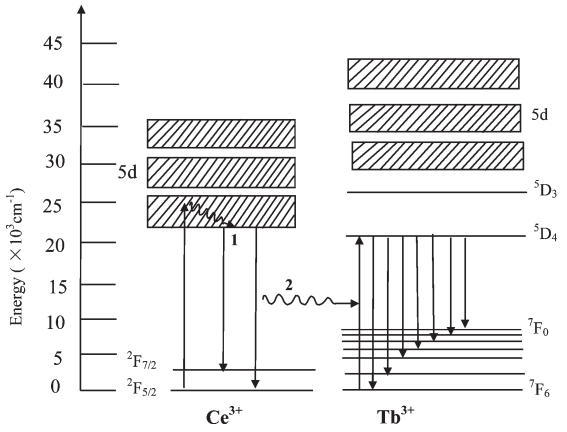

Figure 18. Energy diagram of the luminescence of $RE_2Si_4N_6C:Ce^{3+}$, Tb^{3+} (RE = Lu, Y) phosphor. 1 indicates the 5d → 4f emission of Ce^{3+} after relaxation from the 5d excitation levels; 2 indicates energy transfer from Ce^{3+} to Tb^{3+} from which $^5D_4 \rightarrow {}^7F_J$ emission occurs.

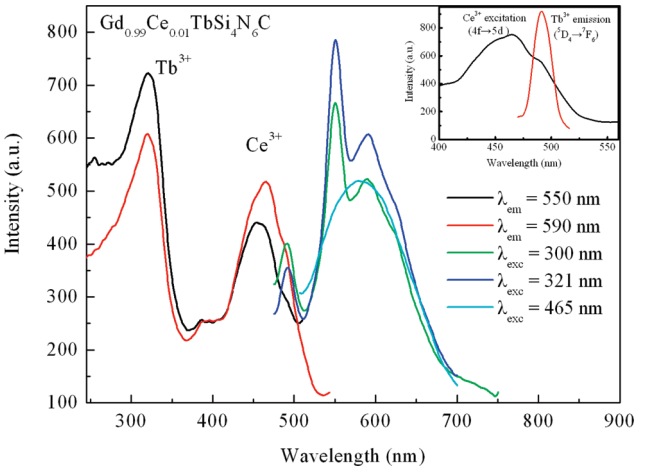

Figure 19. Typical excitation and emission spectra of Ce^{3+}/Tb^{3+}-codoped $Y_2Si_4N_6C$ phosphor. Inset shows the partial overlap between the $^5D_4 \rightarrow {}^7F_6$ emission of Tb^{3+} and the excitation band of Ce^{3+} in $Gd_2Si_4N_6C$ host lattice.

of Tb^{3+}. In Ce^{3+}/Tb^{3+}-codoped $RE_2Si_4N_6C$ (RE = Lu, Y) phosphors, 350−490 nm excitation energies can be absorbed by Ce^{3+} through the 4f → 5d transition. After relaxation the Ce^{3+} ion transfers its excitation energy to the Tb^{3+} ions at short distance which then are pumped to the $^5D_4$ level from which the $^5D_4 \rightarrow {}^7F_J$ (J = 6, 5, 4, 3, 2) emission occurs. Simultaneously, the Ce^{3+} ion may also decay radiatively itself, which results in the 5d → 4f emission of Ce^{3+}, as shown in Figure 18. The energy transfer mechanisms from Ce^{3+} to Tb^{3+} in $RE_2Si_4N_6C:Ce^{3+}$, Tb^{3+} (RE = Lu, Y) phosphors are different from those observed in some other Ce^{3+}/Tb^{3+}-codoped phosphors, such as $CeMgAl_{10}O_{19}:Tb^{3+}$, $GdMgB_5O_{10}:Ce^{3+},Tb^{3+}$, $LaPO_4:Ce^{3+},Tb^{3+}$,[30,36−38] $MSO_4:Ce^{3+},Tb^{3+}$ (M = Ca, Sr, and Ba),[39] $CeF_3:Tb^{3+}$,[40] $Ca_3Y_2(Si_3O_9)_2:Ce^{3+},Tb^{3+}$,[41] $Ca_2Al_2SiO_7:Ce^{3+},Tb^{3+}$,[42] and so forth. In these phosphors, the UV light is absorbed by the 5d bands of Ce^{3+} at higher energies, which then transfers its energy to the 4f levels, that is, $^5D_3$, $^5L_{10}$, and higher energy levels of Tb^{3+}, finally resulting in mainly $^5D_4 \rightarrow {}^7F_J$ green emission. The energy transfer mechanisms from Ce^{3+} to Tb^{3+} in $RE_2Si_4N_6C:Ce^{3+}$, Tb^{3+} (RE = Lu, Y) are similar to the phenomena observed in $(Sr,Ba)_2SiO_4:Eu^{2+},Tb^{3+}$[43] and $Ca_5(PO_4)_3Cl:Eu^{2+},Tb^{3+}$ phosphors.[44] In these two phosphors, the Eu^{2+} emission band overlaps with $^7F_6 \rightarrow {}^5D_4$ excitation transition of Tb^{3+} at about 485 nm. As a consequence, the energy transfer from the Eu^{2+} 5d band to the $^5D_4$ energy level of Tb^{3+} occurs.

3.4.2. Energy Transfer from Tb^{3+} to Ce^{3+} in Ce^{3+}/Tb^{3+}-Codoped $Gd_2Si_4N_6C$ Phosphor. The excitation spectrum of Ce^{3+}/Tb^{3+}-codoped $Gd_2Si_4N_6C$ phosphor shows two main bands with peak centers at about 320 and 465 nm (Figure 19). By comparing it with the excitation spectra of the Tb^{3+} and Ce^{3+} singly doped $Gd_2Si_4N_6C$ phosphors, the first excitation band peaking at 320 nm and the second one peaking at 465 nm can be ascribed to the spin allowed 4f → 5d transition of Tb^{3+} and the 4f → 5d transition of Ce^{3+} ions in this host lattice, respectively. Under the direct excitation of the Ce^{3+} absorption bands in the wavelength range of 400−490 nm, the emission spectrum (Figure 19) only shows typical band emission of Ce^{3+} without any line emissions from Tb^{3+}. It means that there is no energy transfer from Ce^{3+} to Tb^{3+} in this phosphor. However, under the direct excitation of Tb^{3+} 4f → 5d excitation band in the wavelength range of 250−350 nm, both strong Ce^{3+} band and Tb^{3+} line emission can be observed. On the basis of the fact that Ce^{3+} ions cannot be

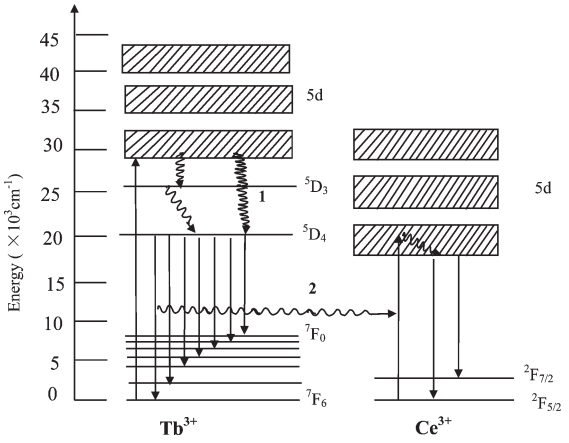

Figure 20. Energy diagram of the luminescence of $Gd_2Si_4N_6C:Ce^{3+}$, Tb^{3+} phosphor. 1 indicates that the $^5D_4 \rightarrow {}^7F_6$ emission of Tb^{3+} after relaxation from the 5d excitation levels; 2 indicates energy transfer from Tb^{3+} to Ce^{3+} from which 5d → 4f emission occurs.

efficiently excited in the wavelength range of 250−350 nm in the Ce^{3+} singly doped $Gd_2Si_4N_6C$ phosphor, we can conclude that there exists energy transfer from Tb^{3+} to Ce^{3+}. As discussed in Section 3.3, due to the larger crystal field strength around Ce^{3+} substituting at a smaller Gd(I) site, the lowest 5d excitation sublevel of Ce^{3+} is located at an even lower energy in $Gd_2Si_4N_6C$ than in $Lu_2Si_4N_6C$ and $Y_2Si_4N_6C$ host lattices, which makes partial overlapping with the $^5D_4 \rightarrow {}^7F_6$ line emission of Tb^{3+} possible (as shown in the inset of Figure 19). As a consequence, a direct energy transfer from the $^5D_4$ energy level of Tb^{3+} to the 5d band of Ce^{3+} would be expected, which is in agreement with the experimental results. As a schematic diagram shown in Figure 20, the lowest 5d excitation sublevel of Ce^{3+} is just situated below the $^5D_4$ energy level of Tb^{3+}. In this phosphor, 250−350 nm excitation energies are absorbed by Tb^{3+} through the spin allowed 4f → 5d transition. After relaxation Tb^{3+} ion transfers its excitation energy to the Ce^{3+} ions which then are pumped to the 5d level from which the 5d → 4f band emission of Ce^{3+} occurs. In the meantime, Tb^{3+} ion also relaxes radiatively, which results in the $^5D_4 \rightarrow {}^7F_J$ line emission of Tb^{3+}, as show in Figure 19. A similar energy transfer from Tb^{3+} to Ce^{3+} has

dx.doi.org/10.1021/cm103495j |*Chem. Mater.* 2011, 23, 1851–1861

already been observed in the Ce^{3+}/Tb^{3+}-codoped YAG phosphor.[45,46] Due to the strong crystal-field splitting effect on the D_2 site in YAG, the 5d excitation band Ce^{3+} is located at a longer wavelength range (i.e., 400−500 nm), which overlaps considerably with the $^5D_4 \rightarrow {}^7F_6$ line emission of Tb^{3+}. As a consequence, the energy transfer from Tb^{3+} to Ce^{3+} occurs in YAG:Ce^{3+},Tb^{3+} phosphor.[45,46]

4. CONCLUSION

$RE_2Si_4N_6C$ (RE = Lu, Y, and Gd) samples were prepared by a solid-state reaction method at high temperature and shown to be isostructural compounds with a space group of *P*21/*c*. Photoluminescence properties of Tb^{3+} and Ce^{3+} singly doped and Ce^{3+}/Tb^{3+}-codoped $RE_2Si_4N_6C$ (RE = Lu, Y, and Gd) phosphors were investigated. Tb^{3+}-activated $RE_2Si_4N_6C$ phosphors emit bright green light under UV excitation around 300 nm corresponding to the $^5D_4 \rightarrow {}^7F_J$ (J = 6, 5, 4, 3) transitions of Tb^{3+}. Because the size of the Gd^{3+} ion is closer to that of the larger dopant Ce^{3+} ion than those of the smaller Lu^{3+} and Y^{3+} ions, the Ce^{3+} ion prefers to occupy the two different Gd(I) and Gd(II) sites simultaneously in Ce^{3+}-doped $Gd_2Si_4N_6C$ phosphor instead of only the larger RE(II) site in Ce^{3+}-doped $RE_2Si_4N_6C$ (RE = Lu, Y) phosphors. In Ce^{3+}-doped $RE_2Si_4N_6C$ (RE = Lu, Y, and Gd) phosphors, the dominant emission is from the $Ce_{RE(I)}$ and $Ce_{RE(II)}$ luminescent centers for RE = Gd versus RE = Lu and Y, respectively, with peak centers at about 535 nm for $RE_2Si_4N_6C$:Ce^{3+} (RE = Lu, Y) and 610 nm for $Gd_2Si_4N_6C$:Ce^{3+}. Due to the high covalency of the silicon−nitride−carbide network, the 4f→5d excitation bands of Tb^{3+} and Ce^{3+} are both located at a lower energy (i.e., longer wavelength range) in these host lattices. Thus, both $RE_2Si_4N_6C$:Tb^{3+} and $RE_2Si_4N_6C$:Ce^{3+} phosphors can be efficiently excited at rather long wavelength. In Ce^{3+}/Tb^{3+}-codoped $RE_2Si_4N_6C$ phosphors, due to the overlap between the Ce^{3+} emission band and the $^7F_6 \rightarrow {}^5D_4$ excitation transition of Tb^{3+}, there exists an energy transfer process from Ce^{3+} to Tb^{3+} in Ce^{3+}/Tb^{3+}-codoped $Lu_2Si_4N_6C$ and $Y_2Si_4N_6C$ phosphors. On the contrary, an energy transfer process from Tb^{3+} to Ce^{3+} is observed in Ce^{3+}/Tb^{3+}-codoped $Gd_2Si_4N_6C$ phosphor resulting from the overlap between the $^5D_4 \rightarrow {}^7F_6$ line emission of Tb^{3+} and the 5d excitation band of Ce^{3+}. Due to the energy transfer from Ce^{3+} to Tb^{3+}, a green Tb^{3+} line emission can be realized by the excitation of highly absorbing Ce^{3+} ions in the visible range (i.e., 390−480 nm) in Ce^{3+}/Tb^{3+}-codoped $RE_2Si_4N_6C$ (RE = Lu, Y) phosphors, demonstrating their high potential for white light LED (backlighting) applications.

■ ASSOCIATED CONTENT

Supporting Information. Diffuse reflection spectra of undoped $RE_2Si_4N_6C$ samples (PDF). This material is available free of charge via the Internet at http://pubs.acs.org.

■ AUTHOR INFORMATION

Corresponding Author

*Tel.: +49-36848-8456. Fax: +49-36848-8490. E-mail: chengjunduan2000@hotmail.com.

■ ACKNOWLEDGMENT

This work was partly supported by the Freistaat Thüringen and the European Union under Contract No. 2008 FE 0070.

■ REFERENCES

(1) Höppe, H. A.; Gunter, K.; Pottgen, R.; Schnick, W. *J. Mater. Chem.* **2001**, *11*, 3300.
(2) Liddell, K.; Thompson, D. P. *J. Mater. Chem.* **2001**, *11*, 507.
(3) Liddell, K.; Thompson, D. P.; Brauniger, T.; Harris, R. K. *J. Eur. Ceram. Soc.* **2005**, *25*, 37.
(4) Liddell, K.; Thompson, D. P.; Teat, S. J. *J. Eur. Ceram. Soc.* **2005**, *25*, 49.
(5) Zhang, H. C.; Horikawa, T.; Machida, K. *J. Electrochem. Soc.* **2006**, *153*, H151.
(6) Li, Y. Q. Ph.D. Thesis, Eindhoven University of Technology, 2005.
(7) Huppertz, H.; Schnick, W. *Angew. Chem., Int. Ed. Engl.* **1996**, *108*, 2115.
(8) Huppertz, H.; Schnick, W. *Z. Anorg. Allg. Chem.* **1997**, *623*, 212.
(9) Huppertz, H.; Schnick, W. *Acta Crystallogr.* **1997**, *C53*, 1751.
(10) Höppe, H. A.; Trill, H.; Kotzyba, G.; Mosel, B. D.; Pottgen, R.; Schnick, W. *Z. Anorg. Allg. Chem.* **2004**, *630*, 224.
(11) Fang, C. M.; Li, Y. Q.; Hintzen, H. T.; de With, G. *J. Mater. Chem.* **2003**, *13*, 1480.
(12) Li, Y. Q.; de With, G.; Hintzen, H. T. *J. Alloys Compd.* **2004**, *385*, 1.
(13) Li, Y. Q.; Fang, C. M.; de With, G.; Hintzen, H. T. *J. Solid State Chem.* **2004**, *177*, 4687.
(14) Kurushima, T.; Gundiah, G.; Shimomura, Y.; Mikami, M.; Kijima, N.; Cheetham, A. K. *J. Electrochem. Soc.* **2010**, *157*, J64.
(15) Schnick, W.; Bettenhausen, R.; Gotze, B.; Hoppe, H. A.; Huppertz, H.; Irran, E.; Kollisch, K.; Lauterbach, R.; Orth, M.; Rannabauer, S.; Schlieper, T.; Schwarze, B.; Wester, F. *Z. Anorg. Allg. Chem.* **2003**, *629*, 902.
(16) Schmidt, P. J.; Jüstel, T.; Höppe, H. A.; Schnick, W. United States Patent US 7611641 B2, 2005.
(17) Starick, D.; Rösler, S.; Hintzen, H. T.; Li, Y. Q. German Patent DE 102005 041 153.3, 2006.
(18) Rodríguez-Carvajal, J. *An Introduction to the Program FullProf 2000*; Laboratoire Lèon Brillouin, CEA-CNRS: Saclay, France, 2001.
(19) Shannon, R. D. *Acta Crystallogr., Sect. A* **1976**, *32*, 751.
(20) Blasse., G.; Bril, A. *Philips Res. Rep.* **1967**, *22*, 481.
(21) Blasse., G. *J. Lumin.* **1970**, *1*, 766.
(22) Robins, D. J.; Cockayne, B.; Lent, B.; Glasper, J. L. *Solid State Commun.* **1976**, *20*, 673.
(23) Shionoya, S.; Yen, W. M. *Phosphor Handbook*; CRC Press LLC: New York, 1999.
(24) Kim, C. H.; Bae, H. S.; Pyun, C. H.; Hong, G. Y. *J. Korean Chem. Soc.* **1998**, *42*, 588.
(25) Hölsä, J.; Leskelä, M. *Phy. Status Solidi B* **1981**, *108*, 797.
(26) Ozawa, L.; Itoh, M. *Chem. Rev.* **2003**, *103*, 3835.
(27) Kang, C. C.; Liu, R. S. *J. Lumin.* **2007**, *122−123*, 574.
(28) Li, Y. Q.; Delsing, A. C. A.; Metslaar, R.; de With, G.; Hintzen, H. T. *J. Alloys Compd.* **2009**, *487*, 28.
(29) Li, Y. Q.; Hirosaki, N.; Xie, R. J.; Takeka, T.; Mitomo, M. *J. Solid State Chem.* **2009**, *18*, 301.
(30) Blasse, G.; Grabmaier, B. C. *Luminescent Materials*; Spring-Verlag: Berlin, 1994.
(31) Kanou, T. *Handbook of Phosphors*; Ohm Press: Tokyo, 1987.
(32) Li, Y. Q.; de With, G.; Hintzen, H. T. *J. Solid State Chem.* **2004**, *177*, 4687.
(33) Toquin, R. L.; Cheetham, A. K. *Chem. Phys. Lett.* **2006**, *423*, 352.
(34) Duan, C. J.; Wang, X. J.; Otten, W. M.; Delsing, A. C. A.; Zhao, J. T.; Hintzen, H. T. *Chem. Mater.* **2008**, *20*, 1597.
(35) Li, Y. Q.; Hirosaki, N.; Xie, R. J.; Takeda, T.; Mitomo, M. *Chem. Mater.* **2008**, *20*, 6704.
(36) Jüstel, T.; Nikol, H.; Ronda, C. R. *Angew. Chem., Int. Ed.* **1998**, *37*, 3084.
(37) Feldmann, C.; Jüstel, T.; Ronda, C. R.; Schmidt, P. J. *Adv. Funct. Mater.* **2003**, *13*, 511.

(38) Srivastave, A. M.; Ronda, C. R. *Electrochem. Soc. Interface* **2003**, 48.
(39) Jose, M. T.; Lakshmanan, A. R. *Opt. Mater.* **2004**, *24*, 651.
(40) Wang, Z. L.; Quan, Z. W.; Jia, P. Y.; Lin, C. K.; Luo, Y.; Chen, Y.; Fang, J.; Zhou, W.; O'Connor, C. J.; Lin, J. *Chem. Mater.* **2006**, *18*, 2030.
(41) Chiu, Y. C.; Liu, W. R.; Yeh, Y. T.; Jang, S. M.; Chen, T. M. *J. Electrochem. Soc.* **2009**, *156*, J221.
(42) Jiao, H. Y.; Wang, Y. H. *J. Electrochem. Soc.* **2009**, *156*, J117.
(43) Hiramatsu, R.; Ishida, K.; Aiga., F.; Fukuda, Y.; Matsuda, N.; Asai, H. *J. Appl. Phys.* **2009**, *106*, 093513.
(44) Zhang, Z.; Wang, J.; Zhang, M.; Zhang, Q.; Su, Q. *Appl. Phys. B: Lasers Opt.* **2008**, *91*, 529.
(45) Turos-Matysiak, R.; Gryk, W.; Grinberg, M.; Lin, Y. S.; Liu, R. S. *Radiat. Meas.* **2007**, *42*, 755.
(46) Liu, X. R.; Wang, X. J.; Wang, Z. K. *Phys. Rev. B* **1989**, *39*, 10633.